Air-Water Flows and Head Losses on Stepped Spillways with Inclined Steps

Arosquipa Nina, Yvan; Shi, Rui; Wüthrich, Davide; Chanson, Hubert

DOI
10.1061/(ASCE)IR.1943-4774.0001701

Publication date
2022

Document Version
Final published version

Published in
Journal of Irrigation and Drainage Engineering

Citation (APA)
Arosquipa Nina, Y., Shi, R., Wüthrich, D., & Chanson, H. (2022). Air-Water Flows and Head Losses on Stepped Spillways with Inclined Steps. *Journal of Irrigation and Drainage Engineering*, *148*(11), Article 04022037. https://doi.org/10.1061/(ASCE)IR.1943-4774.0001701

Air–Water Flows and Head Losses on Stepped Spillways with Inclined Steps

Yvan Arosquipa Nina[1]; Rui Shi[2]; Davide Wüthrich[3]; and Hubert Chanson[4]

Abstract: On a stepped spillway, the staircase invert profile generates some intense turbulent dissipation during the spill, associated with a significant reduction of kinetic energy, as well as strong self-aeration. The present study focused on the effects of inclined downward steps on the air–water flow properties, flow resistance, and head losses because these mostly relate to spillway design. Some physical modeling was conducted in a relatively large facility with a 45° stepped chute (1V:1H) operating with Reynolds numbers $2.8 \times 10^3 < \mathrm{Re} < 1 \times 10^6$. The presence of downward steps induced some elongated asymmetrical cavity shapes, creating a less stable cavity recirculation pattern along the entire chute, leading to different interactions with the main stream. In terms of basic air–water flow properties, the distributions of void fraction and bubble count rate presented very close results for all three stepped geometries, both qualitatively and quantitatively. The interfacial velocities did not reach any uniform equilibrium (i.e., normal flow) condition, and the fastest velocities were recorded with the 1V:2.33H inclined downward stepped chute geometry ($\delta = 23.3°$ and $\lambda/k = 3$), and the slowest velocities on the horizontal stepped chute ($\delta = 0$ and $\lambda/k = 2$). The Darcy-Weisbach friction factor f and relative head loss $\Delta H/H_{\max}$ were estimated in the self-aerated flow. The comparative analyses suggested that the largest total drag and head losses were observed on the stepped chute with flat horizontal steps. An inclined downward stepped design yielded lesser head losses for all investigated flow conditions, providing an important information for practical engineers designing these hydraulic structures. **DOI: 10.1061/(ASCE)IR.1943-4774.0001701.**

Author keywords: Stepped spillways; Inclined steps; Air–water flows; Head losses; Physical modeling.

Introduction

Stepped spillway operations are characterized by a highly turbulent flow, intense free-surface aeration, sometimes referred to as white waters, and high head losses in comparison with smooth chutes (Chanson 1995b; Novak et al. 1996; Matos and Meireles 2014). Fundamentally, the staircase invert induces flow separation and generates intense turbulent dissipation during the spill, associated with a significant reduction of kinetic energy in the free-surface flow, as well as strong self-aeration (Rajaratnam 1990; Peyras et al. 1992; Chanson et al. 2015). The self-aeration on stepped chutes has been investigated in the laboratory since the mid-1990s (Ruff and Frizell 1994; Chamani and Rajaratnam 1999; Boes 2000; Matos et al. 2001; Chanson and Toombes 2002a), and the air entrainment and head losses have been extensively studied for configurations with flat horizontal steps (Ohtsu et al. 2004; Gonzalez 2005; Felder 2013; Zhang 2017).

During the design and construction of stepped spillways, the selection of downward step slope might be linked to construction costs, ease of placement, drainage of dam structure, and prevention of water ponding after a flood event (Pravdivets and Bramley 1989; McLean and Hansen 1993). For embankment dam stepped spillways, precast concrete step elements are placed as overtopping protections system, and they are often inclined downward to facilitate the drainage of the protective layer placed between the earthfill material and the elements (Pravdivets 1992). The protective layer functions as a seepage filter to protect the subsoil layers from erosion, with drainage holes typically installed on the steps' vertical faces [Fig. 1(b)].

Very extensive stability analyses were undertaken and supported by both full-scale prototype and laboratory testing, especially some very extensive works in the USSR, UK, and US (Pravdivets and Bramley 1989; Baker and Gardiner 1994; Frizell and Ruff 1995). Precast overlay blocks are typically placed in an overlapping manner [Fig. 1(b)], and the critical stability limit depends on the block shape, weight and drainage. At the Dneipr hydropower plant, precast concrete elements were successfully used with velocities up to 23 m/s and maximum unit discharge of 60 $\mathrm{m^2/s}$ (i.e., $Q_{\max} = 845\ \mathrm{m^3/s}$). Detailed inspections during and after the prototype tests demonstrated no damage, and the prototype pressure measurements indicated that the stability of the concrete step elements was based upon basic fluid dynamics principles and provided the hydrodynamic pressure of the flow itself (Grinchuk et al. 1977). Fig. 1 presents the 48-m-wide stepped spillway of the Bruton flood storage reservoir (UK), with a discharge capacity in excess of 200 $\mathrm{m^3/s}$ (Pether et al. 2009). A related situation is a roller-compacted concrete (RCC) overtopping protection when the steps are trimmed and sloped with a distinct angle, as at Lima Dam in the US (McLean and Hansen 1993). Most applications of inclined steps tend to be small-to medium-size structures shorter than 25–30 m high.

[1]Research Student, School of Civil Engineering, Univ. of Queensland, Brisbane, QLD 4072, Australia.

[2]Ph.D. Student, School of Civil Engineering, Univ. of Queensland, Brisbane, QLD 4072, Australia.

[3]Postdoctoral Research Fellow, School of Civil Engineering, Univ. of Queensland, Brisbane, QLD 4072, Australia; Assistant Professor, Faculty of Civil Engineering and Geosciences, Technical Univ. Delft, Delft 2628, Netherlands. ORCID: https://orcid.org/0000-0003-1974-3560

[4]Professor in Hydraulic Engineering, School of Civil Engineering, Univ. of Queensland, Brisbane, QLD 4072, Australia (corresponding author). ORCID: https://orcid.org/0000-0002-2016-9650. Email: h.chanson@uq.edu.au

Note. This manuscript was submitted on January 20, 2022; approved on April 29, 2022; published online on August 18, 2022. Discussion period open until January 18, 2023; separate discussions must be submitted for individual papers. This paper is part of the ***Journal of Irrigation and Drainage Engineering***, © ASCE, ISSN 0733-9437.

(a) (b)

Fig. 1. Prototype stepped spillways with inclined downward steps for Bruton flood storage reservoir, UK ($\theta = 14°$, $H = 10.75$ m, $B = 48$ m, and $Q \approx 250$ m^3/s): (a) general view of the spillway shortly after completion in 2008; and (b) construction details with installation of precast concrete blocks over the geotextile membrane. (Images courtesy of John Ackers.)

The present study was motivated by a lack of detailed investigations on the effects of step inclination on the air–water flow properties and head losses of the stepped spillway overflow. New experiments were conducted in a relatively large facility across a broad range of Reynolds numbers, i.e., $2.8 \times 10^3 < \text{Re} < 1 \times 10^6$. Detailed visual observations and air–water flow measurements were performed, examining the comparative self-aeration and energy-dissipation performances. Some unique and novel aspects of the present work were the systematic characterization of the effects of inclined steps on the head losses based upon the air–water flow properties, and the relatively high Reynolds number achieved in the largest air–water flow experiment ($\text{Re} = 0.8 \times 10^6$).

Physical Modeling Methodology and Approach

Presentation

In the physical model, the flow conditions must be similar to those in the full-scale hydraulic structure (Novak and Cabelka 1981; Chanson 2004b; Novak et al. 2010). For a rectangular stepped spillway channel, a simplified dimensional analysis leads to a number of dimensionless relationships among the air–water turbulent flow properties, fluid properties, boundary conditions, and channel geometries

$$C, \frac{V}{V_c}, \frac{v}{V_c}, \frac{F \times d_c}{V_c}, \ldots = F_1\left(\frac{x}{d_c}, \frac{y}{d_c}, \frac{z}{d_c}, \frac{d_c}{h}, \rho \times \frac{V \times D_H}{\mu}, \frac{g \times \mu^4}{\rho \times \sigma^3}, \frac{B}{d_c}, \theta, \frac{k_s'}{d_c}, \frac{k}{\lambda}, \ldots\right) \quad (1)$$

where C = void fraction; V = interfacial velocity; v = characteristic velocity fluctuation; F = bubble count rate; d_c and V_c = critical flow depth and velocity, respectively; x, y, and z = longitudinal, normal, and transverse coordinates, respectively; D_H = hydraulic diameter, where $D_H = (4 \times W \times d)/(W + 2 \times d)$; B = channel width; h and l = step height and length respectively; g = gravity acceleration; θ = chute slope; μ = dynamic viscosity of water; ρ = water density; σ = surface tension between air and water; k_s' = equivalent sand roughness height of the step surface; k is the step cavity depth; and λ = step cavity length (Fig. 2).

Eq. (1) includes the dimensionless discharge d_c/h, which is proportional to a Froude number defined in terms of the step height h, i.e., $d_c/h = [q^2/(g \times h^3)]^{1/3}$ where q is the water discharge per unit width, $q = Q/B$. Herein, the same fluids were used in model and prototype, thus yielding an additional constraint, i.e., a constant Morton number (Wood 1991; Pfister and Chanson 2012). More, the chute slope ($\tan\theta = h/l$) and the channel width B were kept

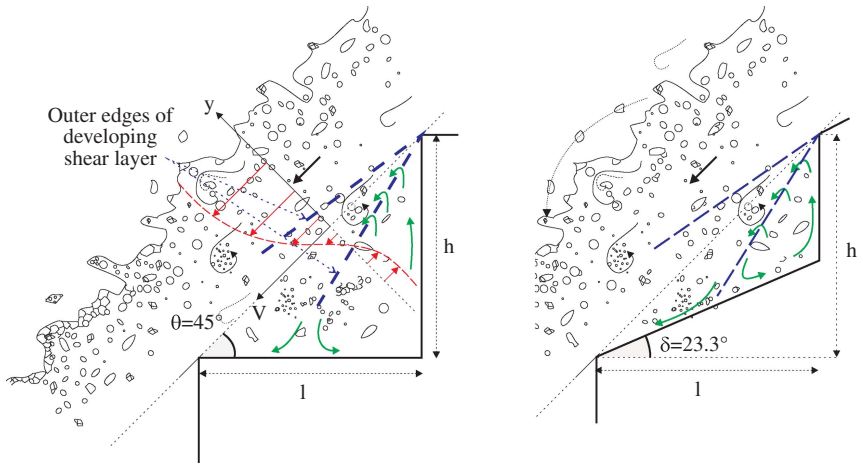

Fig. 2. Definition sketch of air–water flow down a 45° stepped chute and cavity recirculation with horizontal and inclined steps.

constant during the experimental study, i.e., $h/l = 1$ and $B = 0.985$ m, and all the measurements were conducted on the channel centerline ($z/B = 0.5$) with smooth steps ($k_s' \approx 0$). Thus, Eq. (1) may be simplified into

$$C, \frac{V}{V_c}, \frac{v}{V_c}, \frac{F \times d_c}{V_c}, \ldots = F_2\left(\frac{x}{d_c}, \frac{y}{d_c}, \frac{d_c}{h}, \rho \times \frac{V \times D_H}{\mu}, \frac{k}{\lambda}, \ldots\right) \quad (2)$$

A Froude and Morton similitude was applied, and the new physical experiments were undertaken in a large-size facility with $h = 0.10$ m operating at large Reynolds numbers, i.e., $2.8 \times 10^3 < \mathrm{Re} < 1 \times 10^6$. The laboratory conditions may correspond to a 1:2 to 1:3 scale study of the stepped spillway designs shown in Fig. 1, thus ensuring the extrapolation of the physical data to full-scale prototypes with negligible scaling effects.

Physical Facility and Instrumentation

New physical experiments were conducted in a facility previously used by Zhang (2017) and Arosquipa Nina et al. (2020) [Fig. 3(a)], $\alpha = 22°$ and $\alpha = 26.6°$. The water was supplied to a 1.7-m-deep and 5-m-wide intake basin through a two-dimensional diffuser, followed by baffles and two series of flow straighteners leading to a 2.8-m-long sidewall convergent with a 5.08:1 contraction ratio, resulting in a smooth and waveless flow in the 0.985-m-wide test section. The stepped chute flow was controlled by an upstream broad-crested weir. The weir was 0.60 m long, 0.985 m wide, and 1.2 m high, with a vertical upstream wall, and upstream and downstream rounded corners. The broad-crested weir was followed by 12 impervious flat steps. Each step was 0.1 m high, 0.1 m long, and 0.985 m wide. The stepped chute ended onto a flat horizontal tailrace channel.

The flow rate was supplied by three pumps controlled by an adjustable alternate current (AC) motor drive with a capacity in excess of 0.35 m^3/s. The water discharge was deduced from the measured upstream head above the broad crest using the discharge calibration results of Zhang and Chanson (2016) as follows:

$$\frac{Q}{B} = \left(0.8966 + 0.243 \times \frac{H_1}{L_{\mathrm{crest}}}\right) \times \sqrt{g \times \left(\frac{2}{3} \times H_1\right)^3} \quad (3)$$

where H_1 = upstream total head above the crest; and L_{crest} = broad-crested weir length ($L_{\mathrm{crest}} = 0.60$ m).

Three stepped configurations were used [Fig. 3(b)]. The reference stepped geometry had 12 identical flat smooth horizontal steps ($\lambda/k = 2$). Two downward step slope geometries were tested: $\delta = 11.3°$ ($\lambda/k = 2.5$ and 1V:5H) and $\delta = 23.3°$ ($\lambda/k = 3$ and 1V:2.33H). The same constant-step slope was applied to all

(a)

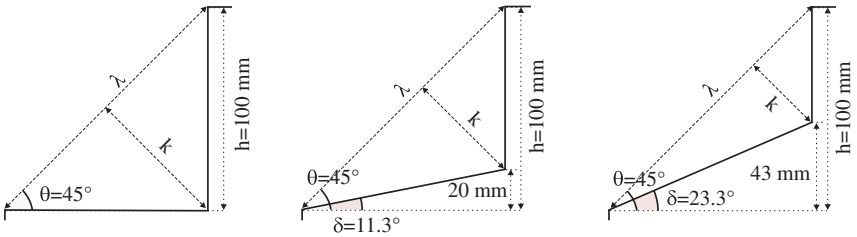

(b)

Fig. 3. Stepped configurations down the 45° (1V:1H) stepped spillway: (a) skimming flow over 1V:5H inclined steps ($\delta = 11.3°$ and $\lambda/k = 2.5$), $d_c/h = 1.6$, $\mathrm{Re} = 8 \times 10^5$, and shutter speed of 1/25 s; and (b) dimensioned undistorted sketch of horizontal and inclined downward steps.

Table 1. Summary of changes in stepped chute flow regimes on flat horizontal and inclined-stepped chutes: comparison with stepped chutes with similar relative cavity aspect ratio λ/h

References	θ (degrees)	B (m)	h (m)	λ/k	Configuration	d_c/h NA-TR	d_c/h TR-SK
Present study	45.0	0.985	0.10	2.0	Flat horizontal steps	0.3	0.95
				2.5	11.3° (1V:5H) step slope	0.3	0.85
				3.0	23.3° (1V:2.33H) step slope	0.3	0.80
Zhang (2017)	45.0	0.985	0.10	2.0	Flat horizontal steps	0.4	0.9
Felder (2013)	26.6	1.0	0.10	2.5	Flat horizontal steps	0.53	1.03
Chanson and Toombes (2002a)	21.8	1.0	0.10	2.9	Flat horizontal steps	0.5	1.0
	15.9	1.0	0.10	3.8	Flat horizontal steps	0.75	1.3

Note: d_c = critical flow depth; h = vertical step height measured from step edge and step edge; k = step cavity depth measured normal to the pseudobottom formed by the step edges; λ = step cavity length measured along the pseudobottom formed by the step edges; θ = slope between pseudobottom formed by step edges and horizontal; NA = nappe flow regime; SK = skimming flow regime; and TR = transition flow regime.

the steps for a given geometry. The horizontal steps were made of PVC. The downward step slopes were manufactured in aluminum plates supported by marine ply wedges, with similar roughness as PVC.

Detailed air–water measurements were performed with dual-tip phase-detection probes (Ø = 0.25 mm). The probes were manufactured at the University of Queensland and excited by an electronic air bubble detector with a response frequency greater than 100 kHz. The separation of probe tips was $\Delta x_{tip} = 6.2$ mm in the longitudinal direction and $\Delta z_{tip} \sim 1.35$ mm in the transverse direction. Similar dual-tip conductivity probes were previously used in a number of air–water flow studies (Chanson and Carosi 2007; Felder and Chanson 2009; Zhang 2017). The phase-detection probe signals were sampled at 20 kHz per sensor for 45 s. The selection of the sampling rate and duration was derived from previous sensitivity analyses (Felder and Chanson 2015).

The main parameters extracted from the signal processing were the void fraction C, bubble frequency F, interfacial velocity V, turbulent intensity Tu, and bubble chord time (Chanson 2002). The dual-tip phase-detection probe measures the change in conductivity between air and water, yielding two quasi-square-wave signals with 0 in water and 1 in air. The signal analysis of the leading sensor gave the time average void fraction, the bubble count rate defined as the number of detected bubbles per second, and the bubble chord-size distributions.

A correlation analysis between the leading and trailing tip signals provided the interfacial velocity and turbulence intensity. The former was the ratio of separation distance between the sensors to the interface travel to the most common interface travel time. The latter was deduced from the broadening of the cross-correlation function compared with the autocorrelation function (Crowe et al. 1998; Chanson 2002). All air–water flow measurements were conducted on the channel centerline. The translation of the probe in the y-direction perpendicular to the pseudoinvert formed by the step edges was controlled by a fine adjustment traverse mechanism connected to a HAFCO (Brisbane, Australia) digital scale unit. The error on the y-position of the probe was less than 0.1 mm.

Visual observations were documented with a digital single lens reflex (dSLR) Pentax K-3 (Tokyo), a digital camera Sony RX100M5A (Tokyo), and a digital camera Casio EX-10 Exilim (Tokyo).

Experimental Flow Conditions

The visual observations were conducted for dimensionless discharges d_c/h between 0.037 and 1.83 corresponding to Reynolds numbers between 2.8×10^3 and 9.7×10^5 for all three stepped configurations. Detailed air–water flow measurements were performed with all three stepped configurations for dimensionless discharges d_c/h between 0.7 and 1.6, corresponding to Reynolds numbers between 2.3×10^5 and 8.0×10^5. The air–water flow measurements focused on the skimming flow regime, most common on modern stepped spillways operating at medium to large discharges.

Flow Patterns

The visual observations were conducted for all three step configurations for $0.037 < d_c/h < 1.83$. Video movies are presented in the Supplemental Materials (Table S1). For all stepped geometries and for increasing discharges, the well-understood stepped chute flow regimes were observed, i.e., nappe, transition, and skimming flow regimes. Simply, the inclined steps did not change the observed flow regimes, although the thresholds between flow regimes were slightly different (Table 1).

At low flow rates ($d_c/h < 0.3$), a nappe flow regime was observed, with a series of small free-falls impacting onto the downstream step. Within the investigated flow conditions ($0.037 < d_c/h < 0.3$), the nappe flow was Type NA3, i.e., without hydraulic jump, for all step geometries (Chanson 1995b). The energy dissipation took place in the form of jet breakup in air and jet impact onto the downstream step face. For intermediate discharges ($0.3 < d_c/h < 0.85$ to 0.95), some intense splashing and hydrodynamic instabilities were seen, i.e., the transition flow regime. The transition flows presented a pseudochaotic flow motion associated with significant spray and a very rough free-surface. As previously reported (Chanson and Toombes 2004), the transition flow regime exhibited important streamwise variations of the flow properties at each step cavity as well as across successive step cavities, being evidences of hydrodynamic flow instabilities that should be avoided whenever possible. For larger discharges ($d_c/h > 0.85$ to 0.95), the flow skimmed over the pseudobottom formed by the step edges as a coherent stream. Movies S1, S2, and S3 (Supplemental Materials and Table S1) illustrate some skimming flow down the stepped chute with horizontal ($\delta = 0$ and $\lambda/k = 2$), 1V:5H ($\delta = 11.3°$ and $\lambda/k = 2.5$), and 1V:2.33H ($\delta = 23.3°$ and $\lambda/k = 3$) inclined steps, respectively. In Movie S1, the upstream skimming flow was nonaerated, and self-aeration was seen developing along the stepped chute. Underneath the pseudobottom formed by the step edges, a strong cavity recirculation motion was maintained through some continuous transfer of momentum from the main stream to the cavity recirculation fluid, although a cavity ejection and replenishment process was irregularly observed. In both transition and skimming flows, the upstream flow was clear water, and white waters took place downstream of the inception point

of free-surface aeration (discussed subsequently), where the flow was strongly aerated [Fig. 3(a)].

The two inclined downward step configurations showed similar basic flow regimes to the flat stepped geometry. With increasing step slope, the step cavity become more oblong and the cavity aspect ratio λ/k increased (Fig. 2 Right), with the ratio λ/k of cavity length to depth tending to an infinite value for a smooth chute. Noteworthy, the change in cavity shape and reduction in cavity size, associated with the step slope, seemed to affect the motion of recirculating fluid and tended to destabilize the cavity recirculation, with different interaction with the skimming flow (Movies S2 and S3 and Table S1). For all step configurations and all discharges, visual observations and video movies showed that the cavity recirculation process was three-dimensional in skimming flows, as reported by Matos (2001). All the observations indicated that the step cavities were highly aerated downstream of the inception of free-surface aeration, and some light cavity aeration was observed one to two step cavities upstream of the inception point.

The current observations of change in flow regimes are presented in Table 1, where the findings are compared with some observations on flat horizontal step configurations, with the same step height $h = 0.10$ m and comparable step aspect ratio λ/k and chute breadth B. Overall, the present observations were close to the literature, although the change from transition to skimming flow occurred at a slightly lower discharge for inclined steps (Table 1). It is believed that the inclined-downward step slope reduced the impact/stagnation pressure on the step face and facilitated the occurrence of a skimming flow pattern at lower flow rates.

Inception of Free-Surface Aeration

At the upstream end of a stepped spillway, the free surface was smooth, and no aeration was observed. As an illustration, Movie S3 presents a side view of the skimming flow for $d_c/h = 1.2$ (Supplemental Materials and Table S1). In the movie, the upstream flow is clear. The inception region of free-surface aeration was characterized by strong interactions between the developing flow turbulence and the free surface. For all stepped spillway geometries, the locations of the inception of free-surface aeration were recorded visually for $0.8 < d_c/h < 1.6$. The present definition of the inception region is based upon the onset of aeration (i.e., white waters) at the free surface, to be consistent with prototype observations and laboratory data in nonrectangular chutes. Fig. 4 presents some comparative photographs of the chute overflows for all three step geometries and several dimensionless flow rates d_c/h from 0.8 to 1.6.

Both present and previous observations showed that the visually determined location of inception of aeration moved downstream with increasing flow rate for a given stepped chute geometry. Noteworthy, the reduction in cavity size, associated with the downward step slope, seemed to affect the location of onset of free-surface aeration by shifting it further downstream with increased discharges compared with the reference configuration of flat-horizontal steps (Fig. 5). The present data are presented in Fig. 5, showing the dimensionless location of the inception point L_I/λ as a function of the dimensionless discharge d_c/h, where L_I is the distance between the first step edge and the inception point. For $d_c/h = 1.4$ and 1.5, the onset of free-surface aeration occurred further downstream with the 1V:2.33H step slope ($\delta = 23.3°$ and $\lambda/k = 3.0$) than with the flat horizontal steps ($\delta = 0$ and $\lambda/k = 2.0$). The finding was consistent with the observation of Zhang and Chanson (2018) with trapezoidal step cavities ($\lambda/k = 2.33$).

Air–Water Flow Properties

Void Fraction and Interfacial Velocity

Downstream of the inception point of free-surface aeration, the air–water flow measurements were recorded at all step edges for the three stepped configurations for dimensionless discharges d_c/h between 0.8 and 1.6, with a focus on the skimming flow regime.

The void fraction data showed a rapid and substantial flow aeration downstream of the inception location. The quantitative observations were consistent with the visual observations. At a given cross section, the void fraction data showed a monotonic increase in void fraction with increasing distance from the pseudobottom formed by the step edges (Fig. 6). Fig. 6 shows typical dimensionless distributions of void fractions, with Y_{90} being the characteristic distance normal to the pseudobottom where the void fraction equals $C = 0.90$, and x is the longitudinal distance from the downstream end of the broad-crested weir. In skimming flows, the void fraction data presented a S-profile, which compared well with prior observations and a theoretical solution of the advective diffusion equation for air (Chanson and Toombes 2002a):

$$C = 1 - \tanh^2\left(K' - \frac{1}{2 \times D_o} \times \frac{y}{Y_{90}} + \frac{1}{3 \times D_o} \times \left(\frac{y}{Y_{90}} - \frac{1}{3}\right)^3\right) \quad \text{for } 0 < y < Y_{90} \tag{4}$$

where K' = dimensionless integration constant and assuming a distribution of dimensionless bubble diffusivity D' as follows:

$$D' = \frac{D_o}{1 - 2 \times \left(\frac{y}{Y_{90}} - \frac{1}{3}\right)^2} \tag{5}$$

with both the dimensionless constant D_o and integration constant K' being functions of the depth-averaged C_{mean} only. Eq. (4) is shown in Fig. 6.

The depth-averaged void fraction C_{mean} provided a quantitative assessment of the flow aeration and rate of air entrainment. The longitudinal distributions of depth-averaged void fraction presented a sharp increase in mean void fraction immediately downstream of the inception point of free-surface aeration. There, in the inception region, the stepped spillway flow was rapidly varied, and a rapid flow bulking took place, as discussed by Chamani (2000), Matos (2000), and Zhang and Chanson (2017). Further downstream, the mean void fraction tended to some constant asymptotic value of about $C_{\text{mean}} \approx 0.35$ and 0.4 for skimming flows and transition flows, respectively, although the present chute might not have been long enough to achieve equilibrium.

Previous studies (Matos 2000; Matos and Meireles 2014) suggested that from the downstream end of the rapidly varied region, the mean void fraction tended to increase in a very gradual way in a much longer chute. The present results were obtained for all stepped configurations and close to the observations of Zhang (2017) in the same facility. Overall, the air–water flows over the inclined steps were aerated at a comparable level to the flow on the flat horizontal stepped chute for the same discharge and step location. Yet, there were subtle differences in air–water flow characteristics.

The air diffusivity coefficient was derived from the best fit of the void fraction profiles [Eq. (4)]. The complete data set is reported in Fig. 7. For all stepped configurations, the depth-averaged diffusivity $(D')_{\text{mean}}$ showed a decreasing trend with increasing Reynolds number, where $(D')_{\text{mean}}$ is defined

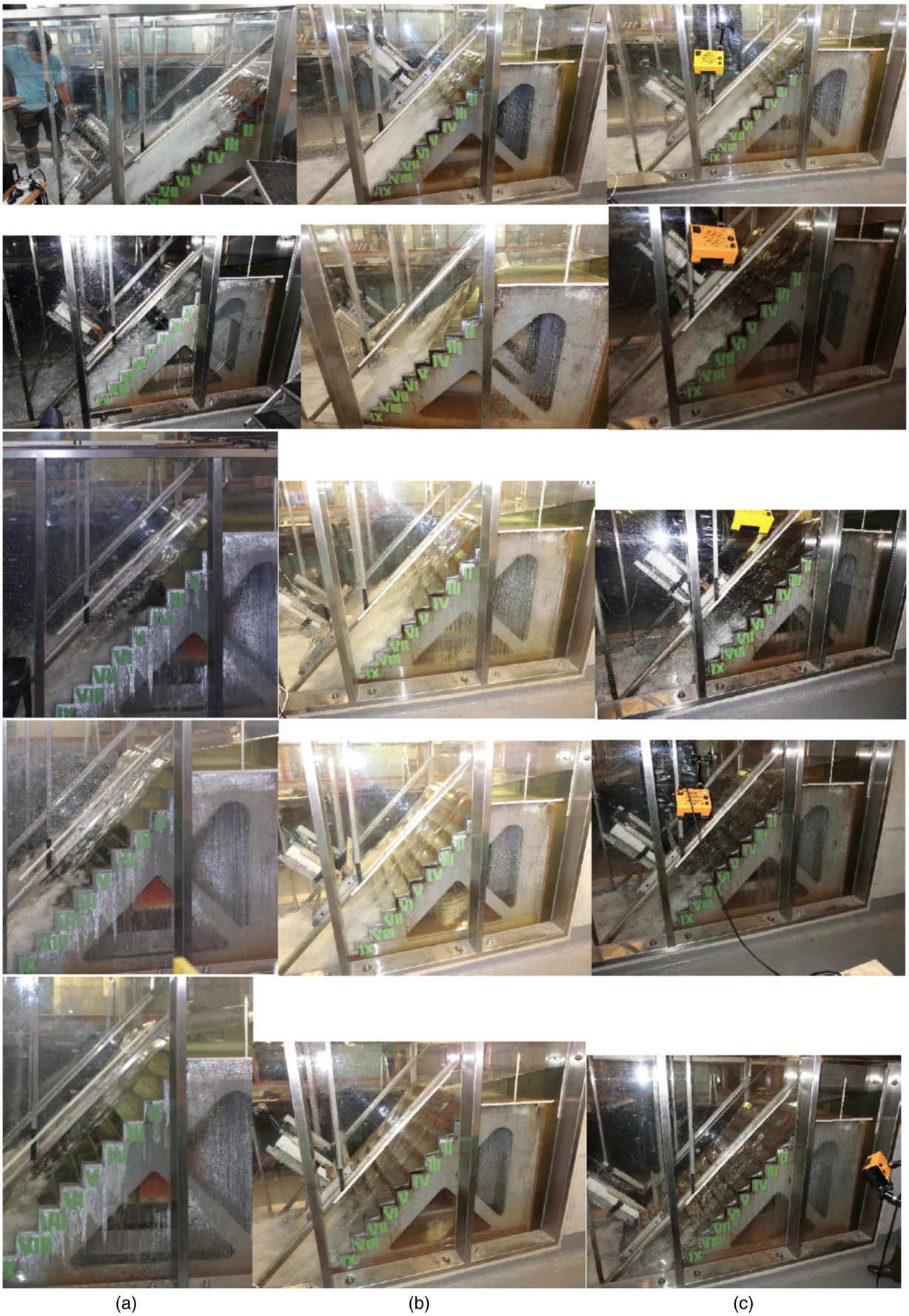

Fig. 4. Effects of the dimensionless discharge on 45° stepped chute with horizontal and inclined steps. From top to bottom: $d_c/h = 0.8$, 1.0, 1.2, 1.4, and 1.6: (a) flat horizontal steps ($\delta = 0$ and $\lambda/k = 2.0$); (b) 1V:5H inclined steps ($\delta = 11.3°$ and $\lambda/k = 2.5$); and (c) 1V:2.3H inclined steps ($\delta = 23.3°$ and $\lambda/k = 3.0$).

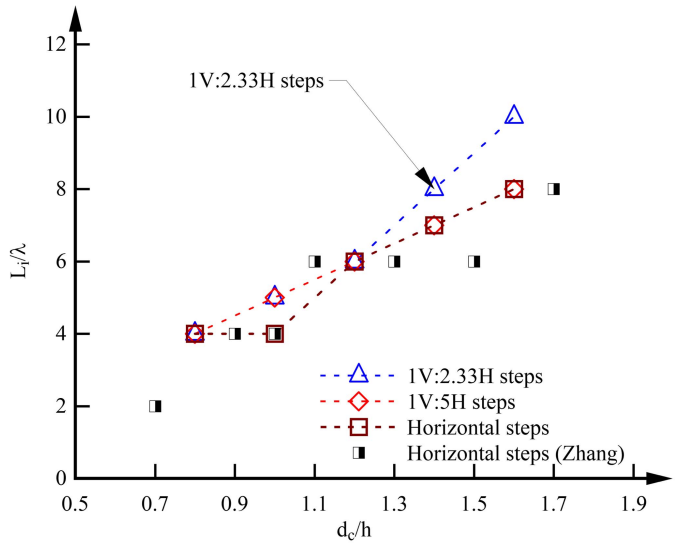

Fig. 5. Location of the inception point of free-surface aeration on a 45° stepped chute with flat horizontal and inclined steps (L_I/λ as a function of d_c/h): comparison with observations by Zhang and Chanson (2016).

$$(D')_{mean} = \frac{1}{Y_{90}} \times \int_{y=0}^{Y_{90}} D' \times dy \quad (6)$$

The trend was likely linked to the downstream shift in inception point location with increasing discharge (Fig. 5), and hence increasing Reynolds number. Overall the current data were correlated by

$$(D')_{mean} = \frac{7.0 \times 10^3}{Re^{0.77}} \quad (7)$$

where Re = Reynolds number defined in terms of the mean velocity and hydraulic diameter, as in the Moody diagram. Eq. (7) applies to all step configurations and skimming flow conditions, and it is plotted in Fig. 7(a).

The diffusivity data are further compared with the literature in Fig. 7(b). Fig. 7(b) presents the dimensionless depth-averaged diffusivity $D_t/(V_{90} \times Y_{90})$, with a comparison between smooth and stepped self-aerated chutes, encompassing smooth laboratory chutes (Straub and Anderson 1958; Aivazyan 1986), smooth prototype chutes (Aivazyan 1986; Cain and Wood 1981), and laboratory stepped chutes (Matos 1999; Boes 2000), where D_t is the air bubble diffusivity and V_{90} is the characteristic air–water velocity measured at $y = Y_{90}$, where $C = 0.9$. Altogether, the data sets suggested that $D_t/(V_{90} \times Y_{90})$ decreased with increasing Reynolds number [Fig. 7(b)]. The observations expanded the previous limited finding of Chanson (1997), and they reinforced earlier conclusions (Chanson 1995a; Zhang and Chanson 2017) showing that a Froude similitude might not be enough to characterize soundly the air diffusion process in smooth and stepped self-aerated chute flows.

The interfacial velocity data were recorded at step edges. Typical interfacial velocity profiles are shown in dimensionless form as V_x/V_c in Fig. 8(a), where V_c is the critical flow velocity. For all stepped configurations, the velocity distributions showed some self-similar profiles that compared favorably to a power law for $y < Y_{90}$, with a constant profile above

$$\frac{V_x}{V_c} = \frac{V_{90}}{V_c} \times \left(\frac{y}{Y_{90}}\right)^{\frac{1}{N}} \quad 0 \le \frac{y}{Y_{90}} \le 1 \quad (8a)$$

$$\frac{V_x}{V_c} = \frac{V_{90}}{V_c} \quad \frac{y}{Y_{90}} \ge 1 \quad (8b)$$

Eq. (8*a*) is shown in Fig. 8(a). In the present study, the velocity power law exponent $1/N$ [Eq. (8*a*)] varied between adjacent step edges for all stepped configurations within $1/9 < 1/N < 1/4.5$. The seesaw fluctuation pattern was believed to be induced by the interferences between developing shear layers in the wake of each step edge and the cavity recirculation motion, previously reported in horizontal step chutes (Carosi and Chanson 2008; Felder and Chanson 2009).

Downstream of the inception point, the self-aerated chute flow did not reach uniform equilibrium: it was gradually-varied and accelerated, as illustrated in Fig. 8(b). The interfacial velocities did not reach some uniform equilibrium (i.e., normal flow) condition. Fig. 8(b) shows the longitudinal distribution of the characteristic air–water velocity V_{90} for the 1V:2.33H inclined stepped chute, with the characteristic air–water velocity V_{90} increasing

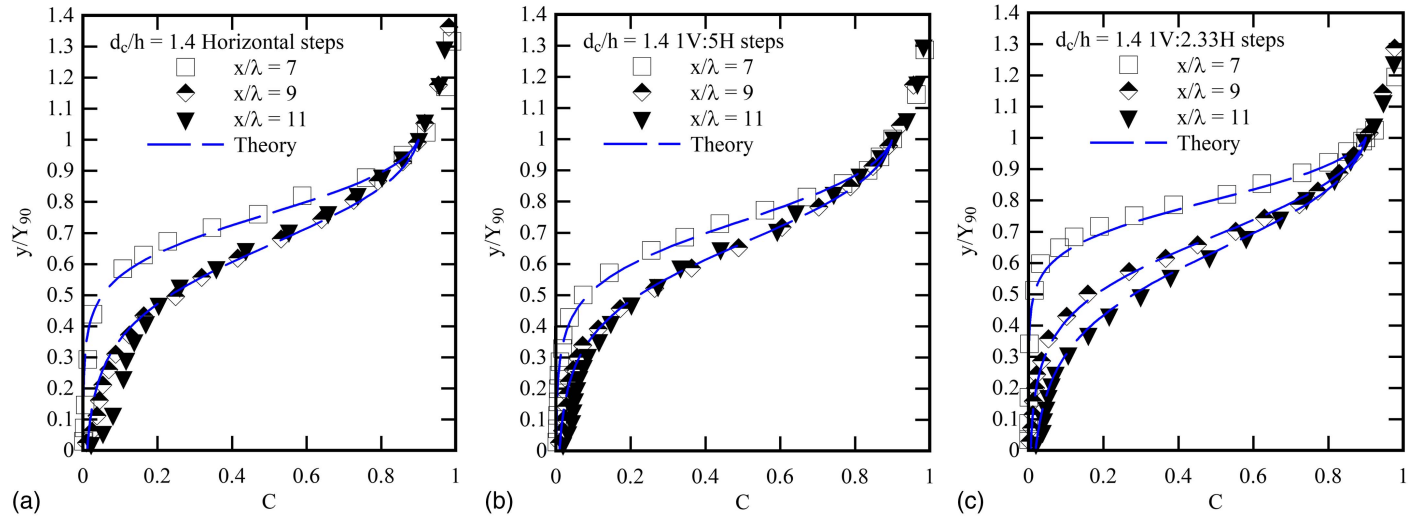

Fig. 6. Dimensionless distributions of void fraction in skimming flow on a 45° stepped chute with horizontal and inclined steps: comparison with advective diffusion theoretical solution [Eq. (4)] (Chanson and Toombes 2002a).

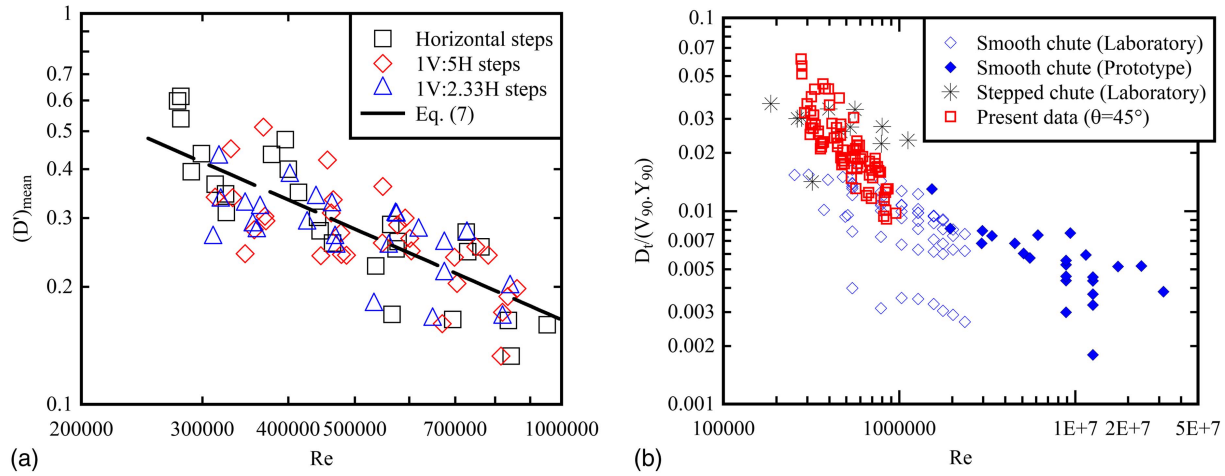

Fig. 7. Dimensionless depth-averaged diffusivities in self-aerated skimming flow on a 45° stepped chute with horizontal and inclined steps as a function of Re in comparison with the literature: (a) dimensionless depth-averaged diffusivity $(D')_{mean}$ in gradually varied self-aerated skimming flow on a 45° stepped chute with horizontal and inclined steps compared with Eq. (7); and (b) dimensionless diffusivity $D_t/(V_{90} \times Y_{90})$ in self-aerated smooth and stepped chute flows.

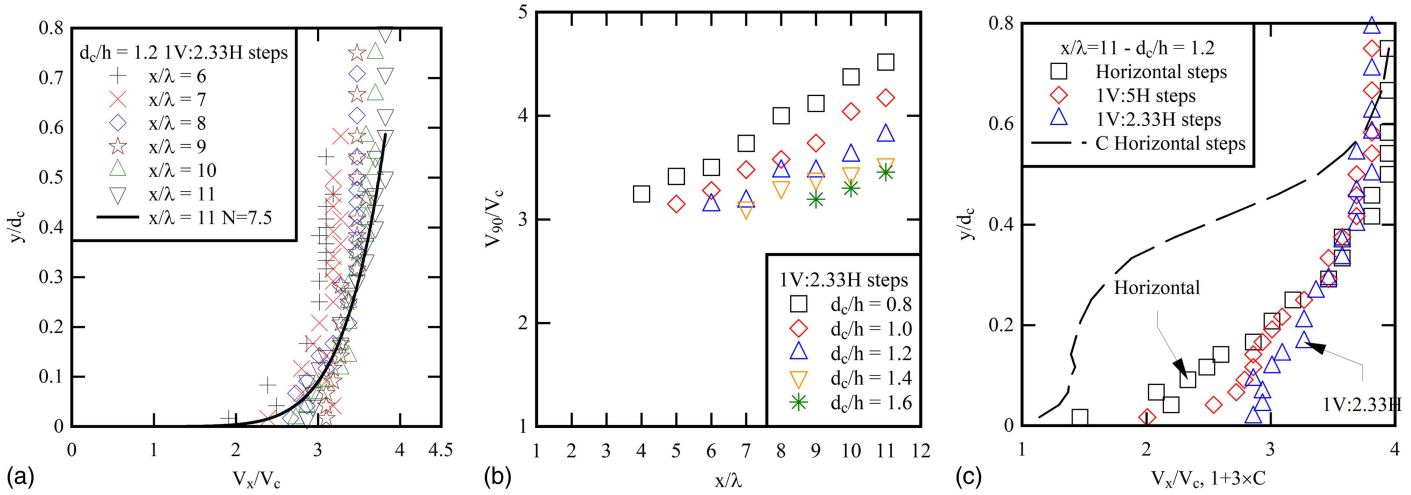

Fig. 8. Dimensionless distributions of interfacial velocities on a 45° stepped chute with horizontal and inclined steps (centerline data at step edges): (a) dimensionless distributions of interfacial velocities V_x/V_c as comparison with Eq. (8*a*) at $x/\lambda = 11$ and flow conditions of $d_c/h = 1.2$, $\mathrm{Re} = 5.2 \times 10^5$, $\theta = 45°$, and $h = 0.10$ m; (b) dimensionless longitudinal distributions of characteristic velocities V_{90}/V_c on a 45° stepped chute with 1V:2.33H inclined steps ($\lambda/k = 3$); and (c) dimensionless distributions of interfacial velocities V_x/V_c at the last step edge as a comparison between horizontal and inclined steps for $d_c/h = 1.2$, as well as void fraction data V for horizontal steps.

monotonically with increasing longitudinal distance. The same trend was observed for the other stepped geometries. At the downstream end of the stepped chute, i.e., $x/\lambda = 11$, the air–water flow measurements indicated that the fastest air–water flow motion was systematically observed with the 1V:2.33H inclined downward stepped chute, with the slowest interfacial velocities on the horizontal stepped chute [Fig. 8(c)]. This is illustrated in Fig. 8(c), showing a typical comparison of the interfacial velocity distributions between the three step configurations.

The turbulence intensity $Tu = v_x'/V_x$ gave some indication of the interfacial velocity fluctuations. Typical data are presented in Fig. 9 in skimming flows. For all stepped configurations, the vertical profile presented a maximum Tu_{max} observed about the location where the bubble count rate was maximum (Fig. 9). At a given cross section, the data showed a monotonic trend with increasing turbulence with increasing bubble count rate, hinting a strong correlation between interfacial turbulence level and air–water flow fragmentation (Chanson and Toombes 2002b; Felder 2013).

Bubble Count Rate and Bubble Sizes

The bubble count rate, sometimes called bubble frequency, is defined as half the number of air–water interfaces detected per second by the leading probe sensor. For a given void fraction, the bubble count rate delivers a quantitative indicator of the air–water flow fragmentation, with increasing fragmentation with an increasing bubble count rate. Typical dimensionless distributions are presented in Fig. 10. For all stepped configurations and investigated flow conditions, the data showed some seminal trends. The vertical distributions presented minima for both a zero void fraction and

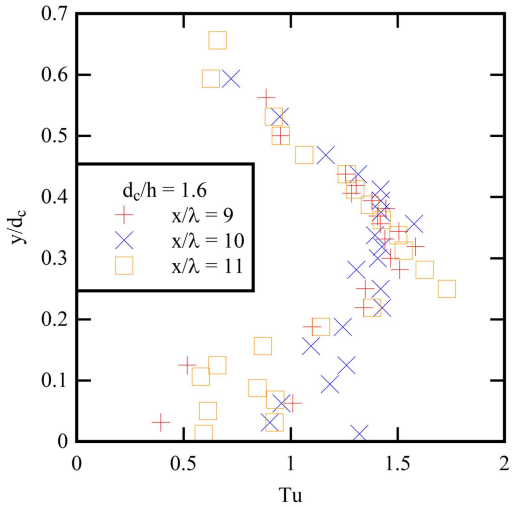

Fig. 9. Dimensionless distributions of interfacial turbulence intensity Tu in skimming flow on a 45° stepped chute with 1V:2.33H inclined steps ($\lambda/k = 3$). Flow conditions are $d_c/h = 1.6$, Re $= 8.0 \times 10^5$, $\theta = 45°$, and $h = 0.10$ m.

very high void fraction ($C = 1$), with a marked maximum in the midair–water column, for local void fractions about 0.3–0.5 (Fig. 10). The bubble count rate increased with increasing distance from the inception point, for a given flow rate and stepped geometry. The findings were close to and similar to earlier investigations in self-aerated smooth and stepped chute flows (Chanson and Toombes 2002a; Gonzalez 2005; Felder 2013).

Although the mean void fraction C_{mean} seemed to achieve some equilibrium value in transition and skimming flows toward the downstream end of the stepped chute, the maximum bubble count rate data exhibited a distinct monotonic increasing pattern without any asymptotic value, clearly illustrated in Fig. 10. The finding was similar to earlier results on stepped chutes across a wide range of chute slopes (Yasuda and Chanson 2003; Gonzalez 2005; Felder 2013; Zhang 2017). Simply, the bubble count rate data indicated a strong fragmentation of the air–water flow, with maximum bubble count rate in excess of 300 bubbles per unit time.

The side-view observations, photographs, and movies showed a range of millimetric bubbles, quantitative measurements of bubble chord lengths are presented herein (Fig. 11). Fig. 11 presents typical normalized probability distribution functions of bubble sizes in the bubbly flow region ($C < 0.3$), recorded at the last step ($x/\lambda = 11$). In each graph, a column represents the probability of bubble/droplet chord length in 0.5-mm intervals, e.g., the probability of chord length from 2.0 to 2.5 mm is represented by the data point labeled 2. The last column corresponds to the probability of chord lengths larger than 20 mm. For all flow conditions and step geometries, the probability of chord length was the largest for particle sizes between 0 and 2 mm. The distributions were, however, skewed, and a nonnegligible amount of particles larger than 5–10 mm were consistently recorded. The probability distribution functions of bubble chords tended to follow a lognormal distribution. Overall, the present data were consistent with previous studies (Chanson and Toombes 2002b; Gonzalez 2005; Felder 2013; Zhang 2017), and very little difference was observed between the three step geometries herein.

Flow Resistance and Head Losses

In skimming flows on a stepped spillway, the total flow resistance is a combination of skin friction along the step faces and of form drag (Rajaratnam 1990; Chanson et al. 2002). In the present study, the friction factor in the air–water flow region was estimated from both momentum and energy considerations, taking into account the air–water flow properties inclusive of the air–water pressure and velocity correction coefficients (Arosquipa Nina et al. 2021). The data are shown as a function of the dimensionless step cavity depth k/D_H in Fig. 12(a), where D_H is the hydraulic diameter.

First, the stepped chute data showed much greater friction factor values than on smooth chutes. Second, irrespective of the method, momentum or energy, the results indicated consistently that the smallest total drag was experienced on the 1V:2.33H ($\delta = 23.3°$) inclined downward stepped chute. On average, f was 20% smaller

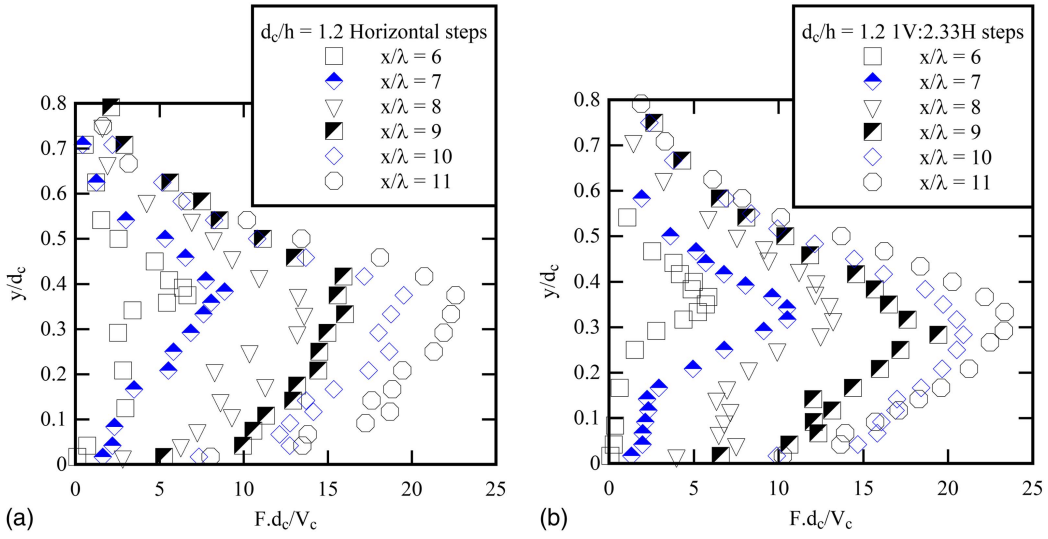

Fig. 10. Dimensionless distributions of bubble count rate $F \times d_c/V_c$ as function of y/d_c in skimming flow on a 45° stepped chute with horizontal and inclined steps with low conditions $d_c/h = 1.2$ and Re $= 5.2 \times 10^5$: (a) horizontal steps ($\delta = 0$ and $\lambda/k = 2$); and (b) 1V:2.33H inclined downward steps ($\delta = 23.3°$ and $\lambda/k = 3$).

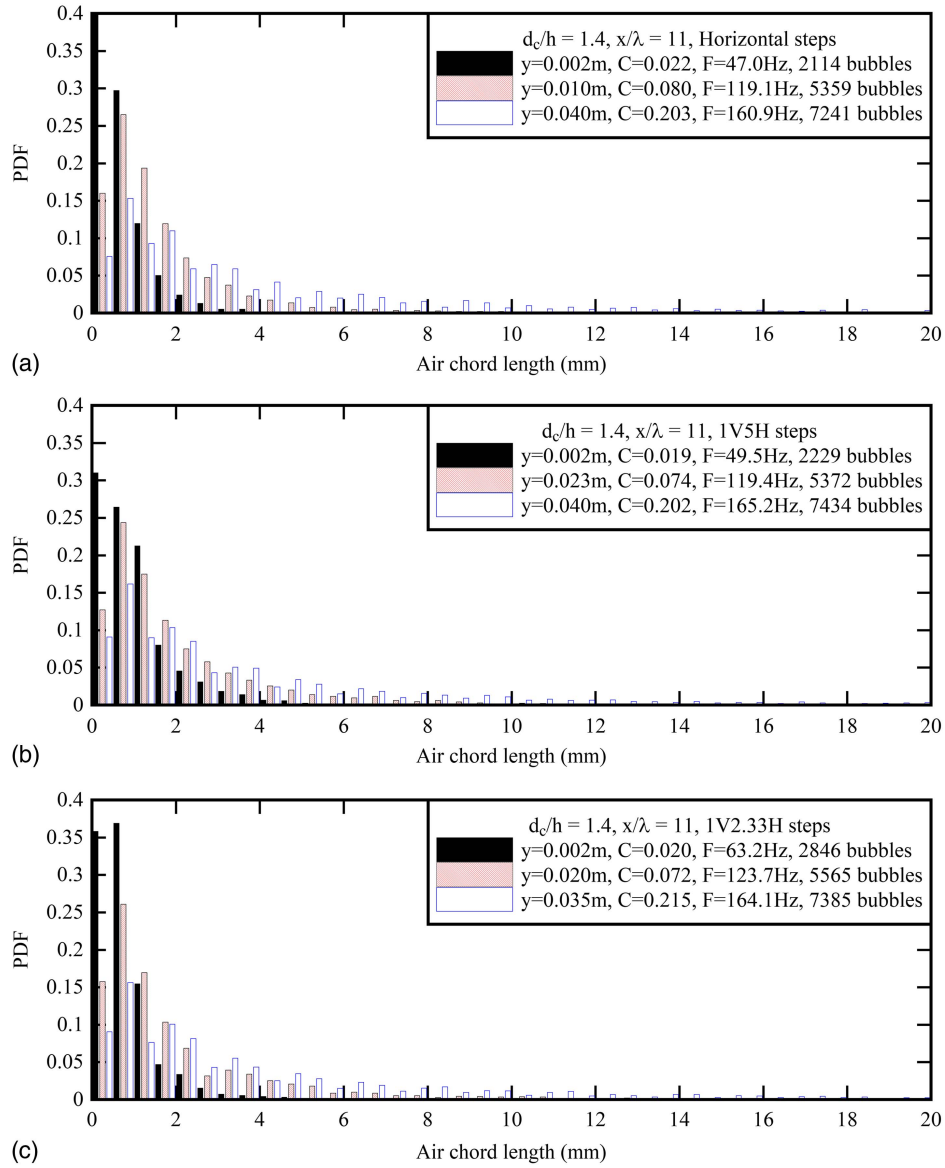

Fig. 11. Normalized probability distribution functions of bubble chord length in the bubbly flow region ($C < 0.3$) of a 45° stepped spillway with horizontal and inclined downward steps with data presented in 0.5-mm intervals for $d_c/h = 1.4$ (skimming flow regime): (a) horizontal steps; (b) 1V:5H inclined steps ($\delta = 11.3°$); and (c) 1V:2.33H inclined steps ($\delta = 23.3°$).

for the 1V:2.33H inclined stepped chute data than for the horizontal stepped chute data. The largest flow resistance on the 45° stepped chute was seen on the horizontal steps.

The current data were further compared with previous air–water flow measurements [Table 2 and Fig. 12(a)]. Although previous data were derived from traditional calculations based upon energy considerations ignoring the air–water velocity and pressure correction coefficients (Arosquipa Nina et al. 2021), the comparison indicated the same magnitude for the dimensionless total drag for all stepped chutes [Fig. 12(a)]. The total drag data compared well with a simplified analytical model of pseudototal boundary shear stress in the mixing layer above a step cavity

$$f_d = \frac{2}{\sqrt{\pi}} \times \frac{1}{K} \tag{9}$$

where $1/K$ = dimensionless expansion rate of the shear layer (Chanson et al. 2002). Eq. (9) predicts $f_d \sim 0.2$ for $K = 6$, close to experimental data, except for a gabion stepped chute [Fig. 12(a)], for which the presence of seepage flow through the steps resulted in a different cavity recirculation process.

The friction factor data are presented in Figs. 12(b and c) as functions of the depth-averaged void fraction C_{mean} measured at the last two step edges. For all step geometries, the data exhibited a trend that suggested a decrease in flow resistance with increasing mean air content, and the friction factors were significantly larger than on self-aerated smooth chutes. In Fig. 12(b), the present data are compared with the reanalyzed data at Aviemore Dam spillway (open circles) (Cain and Wood 1981). The result was basically independent of the step geometry and approach (momentum and energy). Simply, the data implied some drag reduction with increasing mean void fraction, consistent with previous findings on stepped chutes (Boes and Hager 2003; Chanson 2004a; Matos and Meireles 2014). For the present data sets, the reduction in total drag may be approximated

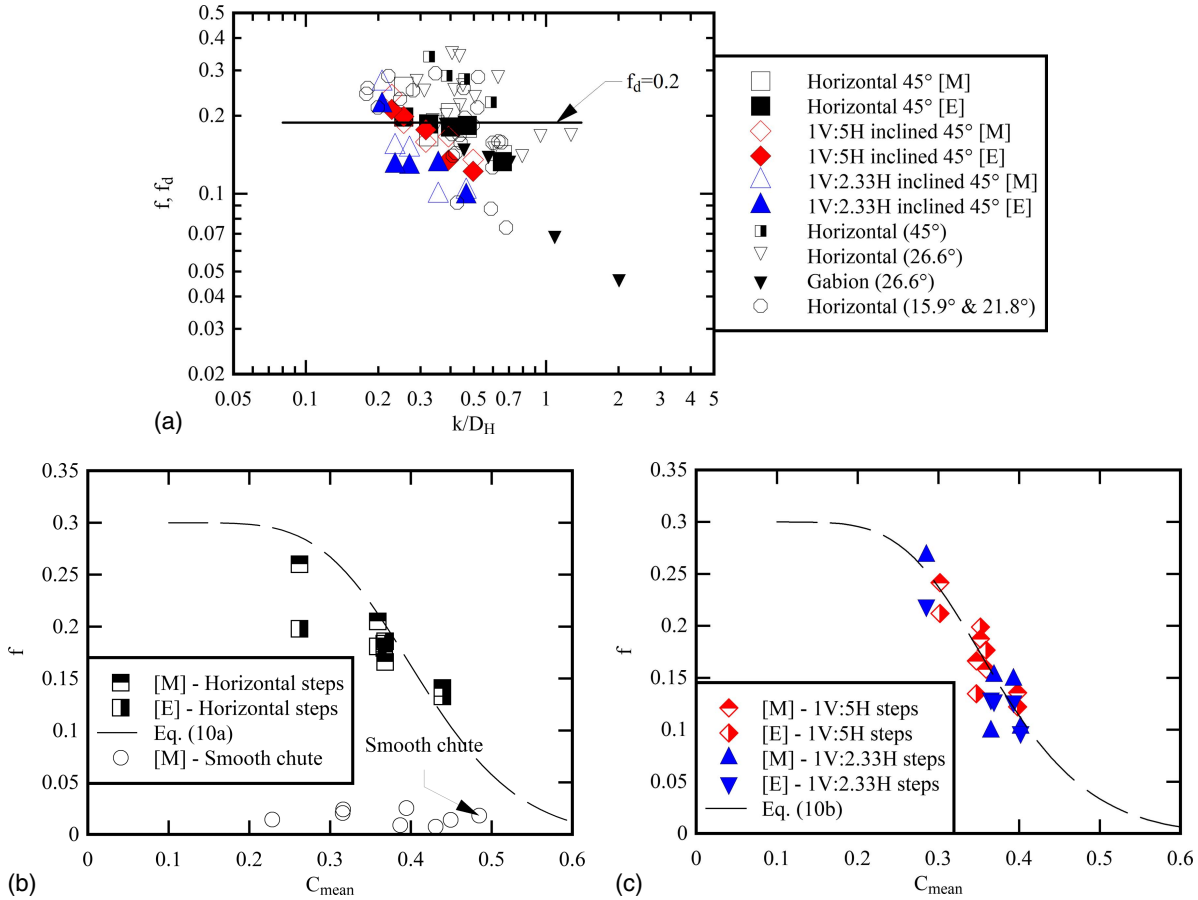

Fig. 12. Flow resistance in air–water skimming flows on a 45° stepped chute with horizontal and inclined steps ($\theta = 45°$ and $h = 0.10$ m) based upon momentum M and energy E considerations: (a) Darcy-Weisbach friction factor as a function of the relative cavity depth k/D_H in comparison with the stepped chute literature (Table 2) and Eq. (9) for $K = 6$ (stepped chutes); (b) friction factor as a function of the depth-averaged void fraction C_{mean} for horizontal steps incomparison with Eq. (10*a*) and smooth chute data at Aviemore Dam spillway; and (c) friction factor as a function of the depth-averaged void fraction C_{mean} for inclined steps in comparison with Eq. (10*b*).

Table 2. Flow resistance in self-aerated stepped chutes: experimental data sets

θ (degrees)	λ/k	h (m)	Geometry	References
45.0	2	0.10	Horizontal steps	Current study[a]
	2.5		1V:5H inclined steps	
	3		1V:2.33H inclined steps	
45.0	2	0.10	Horizontal steps	Zhang (2017)[b]
26.6	2.5	0.10	Horizontal steps	Wuthrich and Chanson (2014)[b], Guenther et al. (2013)[b], and Chanson and Felder (2010)[b]
			Gabion horizontal steps	Wüthrich and Chanson (2014)[b]
21.8	2.9	0.10	Horizontal steps	Chanson and Toombes (2002a)[b] and Carosi and Chanson (2008)[b]
		0.05		Felder and Chanson (2009)[b]
15.9	3.9	0.10	Horizontal steps	Chanson and Toombes (2002a)[b] and Gonzalez (2005)[b]
		0.05		Gonzalez (2005)[b]

[a]Complete calculations based upon momentum and energy considerations taking into account the air–water velocity and pressure correction coefficients.
[b]Traditional calculations based upon energy considerations ignoring the air–water velocity and pressure correction coefficients.

$$f = \frac{0.3}{2} \times \left(1 + \tanh\left(2 \times \frac{0.41 - C_{mean}}{C_{mean} \times (1 - C_{mean})}\right)\right)$$

$\theta = 45°$, horizontal steps (10*a*)

$$f = \frac{0.3}{2} \times \left(1 + \tanh\left(2 \times \frac{0.37 - C_{mean}}{C_{mean} \times (1 - C_{mean})}\right)\right)$$

$\theta = 45°$, inclined downward steps (10*b*)

where tanh = hyperbolic tangent function. Eqs. (10*a*) and (10*b*) are shown in Figs. 12(b and c), respectively. The correlations are rough estimates that satisfy some basic boundary conditions, i.e., f is very small in air flow ($C_{mean} = 1$), and f tends to 0.3 in clear water ($C = 0$). The latter is valid for this chute slope and tested range of dimensionless discharges. Despite some scatter, both trends confirmed Chanson's (1993) early assumption that free-surface aeration induces some total drag reduction in self-aerated skimming flow above a stepped chute.

In skimming flows, separation occurs at each step edge, and a shear layer develops in the wake of the singularity formed by the step edge, with some momentum transfer across the shear zone, from the high-velocity main stream into the cavity, as well as some cavity recirculation motion underneath (Fig. 2). It is suggested that drag reduction results from the interrelationship between bubbles and turbulence in the shear zone and in the step cavity. The small bubbles may block the fluid stretching in the shear zone, leading to vortex inhibition. The reduction in small-scale eddy numbers, and an associated reduction in momentum transfer across the shear layer, might contribute to the total drag reduction. Although the process is affected by the cavity shape and recirculation motion, the process is strongly related to the air bubbles' convection in the shear layer and their interactions with the vortical structures and pairing.

Head Losses

The head losses above the stepped chute is a key parameter, e.g., to design a downstream stilling basin. In the current study, the total head loss ΔH was then calculated

$$\Delta H = H_{max} - H_{res} \quad (11)$$

where H_{max} = upstream head above the sampling location, i.e., the upstream reservoir head; and H_{res} = residual head at the last step edge, calculated based upon the air–water flow properties. The relative head losses $\Delta H/H_{max}$ expressed the percentage of total head losses along the entire stepped chute, including both the developing clear-water flow region and aerated flow region. The total head loss data are reported in Fig. 13 in terms of dimensionless head losses $\Delta H/H_{max}$ at the downstream end of the chute, i.e., $x/\lambda = 11$. The data are presented as functions of the dimensionless drop in elevation $\Delta z_o/d_c$ between the broad-crested weir and the sampling location.

The present experimental results showed that the 1V:2.33H inclined stepped chute was the least efficient in terms of energy dissipation. The horizontal stepped configuration ($\delta = 0$ and $\lambda/k = 2$) yielded the largest relative head losses, with intermediate results for the 1V:5H inclined stepped chute ($\delta = 11.3°$ and $\lambda/k = 2.5$). The difference between horizontal steps and 1V:2.33H inclined steps was in average 12% in terms of total head loss at the downstream end of the chute.

Table 3. Air–water flow measurements on stepped chutes: energy dissipation rate data sets

θ (degrees)	h (m)	λ/k	Geometry	$\Delta z_o/h$	References
45.0	0.10	2	Horizontal steps	11	Current study[a]
		2.5	1V:5H inclined steps		
		3	1V:2.33H inclined steps		
26.6	0.10	2.5	Horizontal steps	9	Wüthrich and Chanson (2014)[b]
			Gabion horizontal steps		
21.8	0.10	2.9	Horizontal steps	7	Chanson and Toombes (2002a)[b]
				9	Carosi and Chanson (2008)[b]
15.9	0.10	3.9	Horizontal steps	7	Chanson and Toombes (2002a)[b]
				9	Gonzalez (2005)[b]

[a]Complete calculations taking into account the air–water velocity and pressure correction coefficients.
[b]Traditional calculations ignoring the air–water velocity and pressure correction coefficients.

The present data were further compared with the air–water flow literature (Table 3) with identical step height in Fig. 13. In comparison, the observations on flatter horizontal stepped chutes with $\theta = 15.9°$ presented the highest relative head losses, whereas the data for $\theta = 21.8°$ and 26.6° gave intermediate results in terms of head losses, with lesser head losses on the 45° stepped chutes (Fig. 13). The large head losses on flatter slopes was possibly linked to the longer chute and longer residence time on the stepped chute, for an identical total drop in elevation, with flatter slopes.

For completeness, observations with a gabion stepped chute are included in Fig. 13. Interestingly, both gabion and inclined step configurations presented some form of resistance to the recirculating motion within the cavity: for the present study, it was the elongated cavity shape; for the gabions, it was the seepage flow coming from the upstream vertical step and the higher roughness of the step surfaces. Nevertheless, the result was a reduced cavity recirculation motion, which led to a lesser head loss.

In summary, the present data indicated a reduction in energy-dissipation performances on stepped chutes with inclined downward steps, compared with a horizontal stepped chute for $\theta = 45°$. Implicitly, the finding implied that form losses were more prominent than skin friction.

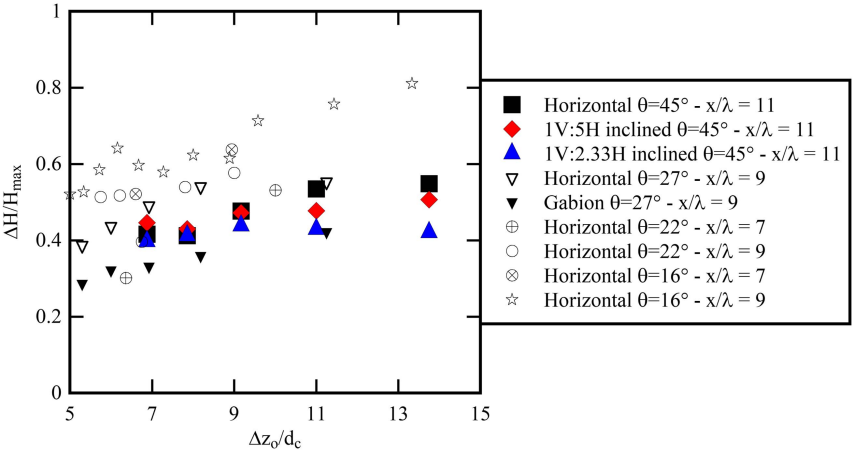

Fig. 13. Relative head losses at the downstream end of a 45° stepped chute with flat horizontal and inclined steps ($\theta = 45°$, $h = 0.10$ m, and $x/\lambda = 11$) in comparison with the literature (Table 3).

J. Irrig. Drain Eng., 2022, 148(11): 04022037

Conclusion

The hydraulic performances of stepped spillway equipped with inclined downward steps were studied with a systematic comparison of the flow properties for $0.4 < d_c/h < 1.8$ ($2.8 \times 10^3 < \mathrm{Re} < 9.7 \times 10^5$) on three step configurations ($0 < \delta < 23.3°$ and $2 < \lambda/k < 3$) on a stepped slope of 45° (1V:1H) and step height of 0.1 m. For each configuration, the flow properties were observed for a wide range of discharges. The presence of a downward step face reduced the cavity size and induced some elongated asymmetrical cavity shape, creating a less stable cavity recirculation pattern along the entire chute, leading to different interactions with the mainstream flow motion. Although the recirculation was three-dimensional for all step geometries, the motion appeared to be more irregular with the elongated cavity shapes for $\delta = 11.3°$ and 23.3° (i.e., $\lambda/k = 2.5$ and 3.0, respectively), compared with that observed with horizontal steps ($\delta = 0$ and $\lambda/k = 2.0$). The downward step slope facilitated a change from transition to skimming flow, with a change occurring at a lower dimensionless flow rate. In skimming flows, the onset of free-surface aeration occurred further downstream with the 1V:2.33H step slope ($\delta = 23.3°$ and $\lambda/k = 3.0$) than with the flat horizontal steps ($\delta = 0$ and $\lambda/k = 2.0$).

In terms of basic air–water flow properties, the distributions of void fraction and bubble count rate presented very close results for all three stepped geometries both qualitatively and quantitatively. The void fraction profiles followed closely theoretical solutions of the advective diffusion equation for air. The diffusivity data showed the same trend for all stepped configurations, i.e., the dimensionless diffusivity decreased with increasing Reynolds number, by a factor of three for the present investigations. The interfacial velocities did not reach any uniform equilibrium (i.e., normal flow) condition, before the end of the chute. The fastest velocities were recorded with the 1V:2.33H inclined downward stepped chute geometry ($\delta = 23.3°$ and $\lambda/k = 3$). At the downstream of the chutes, the average velocities were about 7%–10% larger than the slowest velocities on the horizontal stepped chute ($\delta = 0$ and $\lambda/k = 2$). The interfacial turbulence intensity showed large turbulence levels, with a strong correlation between interfacial turbulence and bubble count rate, hence air–water flow fragmentation and air–water interfacial area. All the bubble count rate distributions presented a marked maximum in a region where the void fraction ranged from 0.30 to 0.50. The maximum bubble count rate increased monotonically along the chute without reaching any asymptotic value. For all flow conditions and step geometries, the probability of chord length was the largest for particle sizes between 0 and 2 mm, and the distributions were skewed, following a lognormal distribution. Altogether, the three tested configurations showed similar two-phase flow behaviors, suggesting that the bubble dynamics within the flow (i.e., number of bubbles and bubble size) seemed to be little affected by the step geometry.

Using both momentum and energy approaches, the Darcy-Weisbach friction factor f and relative head loss $\Delta H/H_{\max}$ were estimated in the self-aerated flow on all three stepped configurations. The comparative analyses indicated that the largest total drag and relative head losses were observed on the stepped chute with flat horizontal steps. The difference was in average 12%. For all investigated flow conditions, the inclined downward stepped design yielded lesser head losses and larger residual heads.

Data Availability Statement

Some or all data, models, or code that support the findings of this study are available from the corresponding author upon reasonable request. These might include the tabular data corresponding to the data presented in Figs. 5–13. Further information has been reported in Arosquipa Nina et al. (2021).

Acknowledgments

The authors would like to thank Professor Jorge Matos (IST Lisbon, Portugal), Dr. Brian Crookston (Utah State University), Professor Daniel Bung (FH Aachen University of Applied Sciences, Germany) and John Ackers for detailed comments and helpful suggestions. They acknowledge some helpful input and advice from Professor David A. Chin (University of Miami). The authors acknowledge the technical assistance of Jason Van Der Gevel and Stewart Matthews (University of Queensland). The financial support of the Swiss National Science Foundation (Grant P2ELP2_181794) and the University of Queensland, School of Civil Engineering is acknowledged.

Notation

The following symbols are used in this paper:

A = clear-water flow area, herein, $A = d \times B$;
B = channel width (m), $B = 0.985$ m in the present study;
C = time-averaged void fraction;
C_{mean} = depth-averaged void fraction, $C_{\mathrm{mean}} = (1/Y_{90}) \times \int_{y=0}^{Y_{90}} C \times dy$;
D_H = hydraulic diameter (m), $D_H = 4 \times A/P_w$;
D_o = dimensionless constant;
D_t = air bubble diffusivity for interfacial aeration (m^2/s);
D' = dimensionless air bubble diffusivity for interfacial aeration;
$(D')_{\mathrm{mean}}$ = depth-averaged dimensionless air bubble diffusivity for interfacial aeration, $(D')_{\mathrm{mean}} = (1/Y_{90}) \times \int_{y=0}^{Y_{90}} D' \times dy$;
d = equivalent clear-water depth (m) in air–water flows, $d = 1/Y_{90} \times \int_{y=0}^{Y_{90}} (1-C) \times dy$;
d_c = critical flow depth (m);
F = bubble count rate (Hz);
f = Darcy-Weisbach friction factor for air–water flow;
f_d = analytical expression of dimensionless total drag;
g = gravity acceleration (m/s^2), $g = 9.794\ \mathrm{m}/\mathrm{s}^2$ in Brisbane, Australia;
H = total head (m);
$H_{\max}$ = maximum head available (m);
H_{res} = residual head (m), defined as the specific energy at the last step edge;
H_1 = upstream head above crest invert (m);
h = vertical step height (m), measured from step edge to step edge;
K = inverse of the dimensionless expansion rate of the shear layer;
K' = dimensionless integration constant;
k = step cavity depth (m) measured perpendicular to the pseudobottom formed by the step edges;
k_s' = equivalent sand roughness height (m);
L_{crest} = crest length (m) in the flow direction: L = 0.60 m herein;
L_I = position (m) of the inception point of free-surface aeration measured from the downstream end of the chute crest;
l = horizontal step length (m);
P_w = wetted perimeter (m);

Q = water discharge (m^3/s);
q = water discharge per unit width (m^2/s): $q = Q/B$;
Re = Reynolds number defined in terms of the mean velocity and hydraulic diameter, $Re = \rho \times (V_{mean} \times D_H)/\mu$;
Tu = interfacial turbulence intensity;
V = velocity (m/s);
V_c = critical flow velocity (m/s), $V_c = (g \times Q/B)^{1/3}$;
V_{mean} = cross-sectional mean velocity (m/s), $V_{mean} = Q/A$;
V_x = longitudinal velocity component (m/s);
V_{90} = characteristic air–water velocity (m/s) where $C = 0.90$;
v = velocity fluctuation (m/s);
x = longitudinal distance (m) positive downstream;
Y_{90} = characteristic air–water elevation (m) where $C = 0.90$;
y = normal distance (m) measured perpendicular to and above the invert or pseudoinvert formed by the step edges;
z = transverse distance (m) from the left sidewall;
z_o = invert elevation (m);
ΔH = total head difference (m);
δ = angle between inclined downward step face and horizontal;
λ = step cavity length (m) measured along the pseudo-bottom formed by the step edges: $\lambda = (h^2 + l^2)^{1/2}$;
μ = dynamic viscosity (Pa·s) of water;
θ = angle between longitudinal invert slope and horizontal;
ρ = water density (kg/m^3); and
σ = surface tension (N/m) between air and water.

Supplemental Materials

Table S1 and Movies S1–S3 are available online in the ASCE Library (www.ascelibrary.org).

References

Aivazyan, O. M. 1986. "Stabilized aeration on chutes." *Gidrotekhnicheskoe Stroitel'stvo* 1986 (12): 33–40.

Arosquipa Nina, Y., R. Shi, D. Wüthrich, and H. Chanson. 2021. *Intrusive and non-intrusive air-water measurements on stepped spillways with inclined steps: A physical study on air entrainment and energy dissipation*. Brisbane, Australia: Univ. of Queensland.

Arosquipa Nina, Y., D. Wüthrich, and H. Chanson. 2020. "Air-water flows on stepped spillways with inclined steps." In *Proc., 22nd Australasian Fluid Mechanics Conf. AFMC2020*. Brisbane, Australia: Univ. of Queensland.

Baker, R., and K. Gardiner. 1994. "The construction and performance of a wedge block spillway at brushes clough reservoir." In *Proc., 8th Conf. British Dam Society*, 214–223. London: Thomas Telford.

Boes, R. M. 2000. "Zweiphasenströmung und Energieumsetzung an Grosskaskaden ('Two-Phase Flow and Energy Dissipation on Cascades.')" Ph.D. thesis, Mitteilungen der Versuchsanstalt fur Wasserbau, Hydrologie und Glaziologie.

Boes, R. M., and W. H. Hager. 2003. "Hydraulic design of stepped spillways." *J. Hydraul. Eng.* 129 (9): 671–679. https://doi.org/10.1061/(ASCE)0733-9429(2003)129:9(671).

Cain, P., and I. R. Wood. 1981. "Measurements of self-aerated flow on a spillway." *J. Hydraul. Div.* 107 (11): 1425–1444. https://doi.org/10.1061/JYCEAJ.0005761.

Carosi, G., and H. Chanson. 2008. "Turbulence characteristics in skimming flows on stepped spillways." *Can. J. Civ. Eng.* 35 (9): 865–880. https://doi.org/10.1139/L08-030.

Chamani, M. R. 2000. "Air inception in skimming flow regime over stepped spillways." In *International workshop on hydraulics of stepped spillways*, 61–67. Zürich, Switzerland: Balkema.

Chamani, M. R., and N. Rajaratnam. 1999. "Characteristics of skimming flow over stepped spillways." *J. Hydraul. Eng.* 125 (4): 361–368. https://doi.org/10.1061/(ASCE)0733-9429(1999)125:4(361).

Chanson, H. 1993. "Stepped spillway flows and air entrainment." *Can. J. Civ. Eng.* 20 (3): 422–435. https://doi.org/10.1139/l93-057.

Chanson, H. 1995a. "Air bubble diffusion in supercritical open channel flow." In *Proc., 12th Australasian Fluid Mechanics Conf. AFMC*. Sydney, Australia: Australasian Fluid Mechanics Society.

Chanson, H. 1995b. *Hydraulic design of stepped cascades, channels, weirs and spillways*. Oxford, UK: Pergamon.

Chanson, H. 1997. *Air bubble entrainment in free-surface turbulent shear flows*. London: Academic Press.

Chanson, H. 2002. "Air-water flow measurements with intrusive phase-detection probes. Can we improve their interpretation?" *J. Hydraul. Eng.* 128 (3): 252–255. https://doi.org/10.1061/(ASCE)0733-9429(2002)128:3(252).

Chanson, H. 2004a. "Drag reduction in skimming flow on stepped spillways by aeration." *J. Hydraul. Res.* 42 (3): 316–322. https://doi.org/10.1080/00221686.2004.9728397.

Chanson, H. 2004b. *The hydraulics of open channel flow: An introduction*. 2nd ed. Oxford, UK: Butterworth-Heinemann.

Chanson, H., D. Bung, and J. Matos. 2015. "Stepped spillways and cascades." In *Energy dissipation in hydraulic structures*. London: CRC Press.

Chanson, H., and G. Carosi. 2007. "Advanced post-processing and correlation analyses in high-velocity air-water flows." *Environ. Fluid Mech.* 7 (6): 495–508. https://doi.org/10.1007/s10652-007-9038-3.

Chanson, H., and S. Felder. 2010. "Energy dissipation on embankment dam stepped spillways, overflow stepped weirs and masonry stepped spillways." In *Proc., 17th Congress of IAHR Asia and Pacific Division*. Madrid, Spain: International Association for Hydro-Environment Engineering and Research.

Chanson, H., and L. Toombes. 2002a. "Air-water flows down stepped chutes: Turbulence and flow structure observations." *Int. J. Multiphase Flow* 28 (11): 1737–1761. https://doi.org/10.1016/S0301-9322(02)00089-7.

Chanson, H., and L. Toombes. 2002b. "Experimental study of gas-liquid interfacial properties in a stepped cascade flow." *Environ. Fluid Mech.* 2 (3): 241–263. https://doi.org/10.1023/A:1019884101405.

Chanson, H., and L. Toombes. 2004. "Hydraulics of stepped chutes: The transition flow." *J. Hydraul. Res.* 42 (1): 43–54. https://doi.org/10.1080/00221686.2004.9641182.

Chanson, H., Y. Yasuda, and I. Ohtsu. 2002. "Flow resistance in skimming flows and its modeling." *Can. J. Civ. Eng.* 29 (6): 809–819. https://doi.org/10.1139/l02-083.

Crowe, C., M. Sommerfield, and Y. Tsuji. 1998. *Multiphase flows with droplets and particles*. London: CRC Press.

Felder, S. 2013. "Air-water flow properties on stepped spillways for embankment dams: Aeration, energy dissipation and turbulence on uniform, non-uniform and pooled stepped chutes." Ph.D. thesis, School of Civil Engineering, Univ. of Queensland.

Felder, S., and H. Chanson. 2009. "Energy dissipation, flow resistance and gas-liquid interfacial area in skimming flows on moderate-slope stepped spillways." *Environ. Fluid Mech.* 9 (4): 427–441. https://doi.org/10.1007/s10652-009-9130-y.

Felder, S., and H. Chanson. 2015. "Phase-detection probe measurements in high-velocity free-surface flows including a discussion of key sampling parameters." *Exp. Therm Fluid Sci.* 61 (10): 66–78. https://doi.org/10.1016/j.expthermflusci.2014.10.009.

Frizell, K. H., and J. F. Ruff. 1995. "Embankment overtopping protection—Concrete blocks or riprap." In *Proc., 1st Int. Conf. on Water Resources Engineering*, 1021–1025. Reston, VA: ASCE.

Gonzalez, C. A. 2005. "An experimental study of free-surface aeration on embankment stepped chutes." Ph.D. thesis, Dept. of Civil Engineering, Univ. of Queensland.

Grinchuk, A. S., Y. P. Pravdivets, and N. V. Shekhtman. 1977. "Test of earth slope revetments permitting flow of water at large specific discharges." *Gidrotekhnicheskoe Stroitel'stvo* 1977 (4): 22–26.

Guenther, P., S. Felder, and H. Chanson. 2013. "Flow aeration, cavity processes and energy dissipation on flat and pooled stepped spillways for embankments." *Environ. Fluid Mech.* 13 (5): 503–525. https://doi.org/10.1007/s10652-013-9277-4.

Matos, J. 1999. "Emulsionamento de ar e dissipação de energia do escoamento em descarregadores em degraus. ('Air entrainment and energy dissipation in flow over stepped spillways.')." Ph.D. thesis, Dept. of Civil Engineering, Instituto Superior Técnico Lisbon.

Matos, J. 2000. "Characteristics of skimming flow over stepped spillways: Discussion." *J. Hydraul. Eng.* 126 (11): 865–869. https://doi.org/10.1061/(ASCE)0733-9429(2000)126:11(865).

Matos, J. 2001. "Onset of skimming flow on stepped spillways: Discussion." *J. Hydraul. Eng.* 127 (6): 519–521. https://doi.org/10.1061/(ASCE)0733-9429(2001)127:6(519.2).

Matos, J., and I. Meireles. 2014. "Hydraulics of stepped weirs and dam spillways: Engineering challenges, labyrinths of research." In *Hydraulic structures and society—Engineering challenges and extremes*. Brisbane, Australia: Univ. of Queensland.

Matos, J., Y. Yasuda, and H. Chanson. 2001. "Interaction between free-surface aeration and cavity recirculation in skimming flows down stepped chutes." In *Proc., 29th IAHR Congress*. Beijing: Tsinghua University Press.

McLean, F. G., and K. D. Hansen. 1993. "Roller compacted concrete for embankment overtopping protection." In *Proc., Special Conf. on Geotechnical Practice in Dam Rehabilitation*. Reston, VA: ASCE.

Novak, P., and J. Cabelka. 1981. "Models in hydraulic engineering." In *Physical principles and design applications*. London: Pitman.

Novak, P., V. Guinot, A. Jeffrey, and D. E. Reeve. 2010. *Hydraulic modelling—An introduction*. London: CRC Press.

Novak, P., A. I. B. Moffat, C. Nalluri, and R. Narayanan. 1996. *Hydraulic structures*. 2nd ed. London: E & FN Spon.

Ohtsu, I., Y. Yasuda, and M. Takahashi. 2004. "Flow characteristics of skimming flows in stepped channels." *J. Hydraul. Eng.* 130 (9): 860–869. https://doi.org/10.1061/(ASCE)0733-9429(2004)130:9(860).

Pether, R., P. Marsh, and P. Cartwright. 2009. "An innovative new spillway for Bruton flood storage reservoir." *Dams Reserv.* 19 (2): 67–72. https://doi.org/10.1680/dare.2009.19.2.67.

Peyras, L., P. Royet, and G. Degoutte. 1992. "Flow and energy dissipation over stepped gabion weirs." *J. Hydraul. Eng.* 118 (5): 707–717. https://doi.org/10.1061/(ASCE)0733-9429(1992)118:5(707).

Pfister, M., and H. Chanson. 2012. "Scale effects in physical hydraulic engineering models: Discussion." *J. Hydraul. Res.* 50 (2): 244–246. https://doi.org/10.1080/00221686.2012.654672.

Pravdivets, Y. P. 1992. "Stepped spillways in world and domestic hydraulic engineering." *Gidrotekhnicheskoe Stroitel'stvo* 10 (Oct): 28–32.

Pravdivets, Y. P., and M. E. Bramley. 1989. "Stepped protection blocks for dam spillways." *Int. Water Power Dam Constr.* 41 (7): 49–56.

Rajaratnam, N. 1990. "Skimming flow in stepped spillways." *J. Hydraul. Eng.* 116 (4): 587–591. https://doi.org/10.1061/(ASCE)0733-9429(1990)116:4(587).

Ruff, J. F., and K. H. Frizell. 1994. "Air concentration measurements in highly-turbulent flow on a steeply-sloping chute." In *Proc., Hydraulic Engineering Conf.* Reston, VA: ASCE.

Straub, L. G., and A. G. Anderson. 1958. "Experiments on self-aerated flow in open channels." *J. Hydraul. Div.* 84 (7): 1890. https://doi.org/10.1061/JYCEAJ.0000261.

Wood, I. R. 1991. "Air entrainment in free-surface flows." In *IAHR hydraulic structures design manual No. 4*. Rotterdam, Netherlands: Balkema.

Wüthrich, D., and H. Chanson. 2014. "Hydraulics, air entrainment and energy dissipation on gabion stepped weir." *J. Hydraul. Eng.* 140 (9): 04014046. https://doi.org/10.1061/(ASCE)HY.1943-7900.0000919.

Yasuda, Y., and H. Chanson. 2003. "Micro- and macro-scopic study of two-phase flow on a stepped chute." In *Proc., 30th IAHR Biennial Congress*, 695–702. Madrid, Spain: International Association for Hydro-Environment Engineering and Research.

Zhang, G. 2017. "Free-surface aeration, turbulence, and energy dissipation on stepped chutes with triangular steps, chamfered steps, and partially blocked step cavities." Ph.D. thesis, School of Civil Engineering, Univ. of Queensland.

Zhang, G., and H. Chanson. 2016. "Hydraulics of the developing flow region of stepped spillways. I: Physical modeling and boundary layer development." *J. Hydraul. Eng.* 142 (7): 8. https://doi.org/10.1061/(ASCE)HY.1943-7900.0001138.

Zhang, G., and H. Chanson. 2017. "Self-aeration in the rapidly- and gradually-varying flow regions of steep smooth and stepped spillways." *Environ. Fluid Mech.* 17 (1): 27–46. https://doi.org/10.1007/s10652-015-9442-z.

Zhang, G., and H. Chanson. 2018. "Effects of step and cavity shapes on aeration and energy dissipation performances of stepped chutes." *J. Hydraul. Eng.* 144 (9): 04018060. https://doi.org/10.1061/(ASCE)HY.1943-7900.0001505.